National Research Journal of Information Technology & Information Science ISSN: 2350-1278
Volume No: 12, Issue No: 2, Year: 2025 (July- December) Peer Reviewed & Refereed Journal (IF: 7.9)
PP: 377-388 Journal Website www.nrjitis.in

ELECTROMAGNETIC PROPAGATION MODELING FOR MM-WAVE ANTENNAS IN 5G SYSTEMS

Shyam Kumar Saphi

Assistant Professor, Department of Physics,

B. M. College, Rahika, Madhubani,

Lalit Narayan Mithila University, Darbhanga (Bihar)

ABSTRACT

Fifth-generation (5G) mobile systems increasingly exploit millimetre-wave (mm-wave) spectrum, especially in the 24–30 GHz and 37–43 GHz bands, to meet stringent capacity and latency requirements. Accurate electromagnetic propagation modelling at these frequencies is essential for the design of phased-array antennas, beamforming strategies and dense small-cell deployments. This study presents a comprehensive discussion of propagation characteristics at mm-wave frequencies, surveys standardised and measurement-based channel models, and develops a hybrid link-level modelling framework combining 3GPP TR 38.901–style large-scale fading with physics-based atmospheric and rain attenuation and realistic antenna array patterns. Using representative 28 GHz urban microcell (UMi) scenarios, we generate numerical results for path loss, additional attenuation due to oxygen absorption and rain, and the impact of beamforming gain on received signal-to-noise ratio (SNR). Data tables and illustrative plots show how link range and reliability depend on environment (LOS/NLOS), frequency, and antenna configuration. The results highlight that, while severe blockage and high basic path loss are inherent at mm-wave, directional beamforming with large arrays and careful link budgeting can deliver viable coverage for 5G access and backhaul, particularly in line-of-sight (LOS) and short-range non-LOS (NLOS) conditions. The proposed modelling framework is generic and can be used to benchmark antenna designs, evaluate deployment strategies, and extend towards emerging 5G-Advanced and early 6G systems.

Keywords: 5G, millimetre-wave, electromagnetic propagation, 28 GHz, 60 GHz, 3GPP TR 38.901, channel modelling, phased arrays, beamforming, rain attenuation.

1. INTRODUCTION

The evolution from LTE to 5G New Radio (NR) has been driven by the need for orders-of-magnitude increases in spectral efficiency, user throughput and connection density, together with ultra-low latency for emerging applications such as immersive media, factory automation and vehicle-to-everything (V2X) communication. A key enabler is the use of spectrum beyond 6 GHz, especially in the so-called FR2 bands around 26–29 GHz, 37–43.5 GHz and 57–71 GHz, where wide contiguous bandwidths are available for mobile access and fixed wireless backhaul [1].

At these frequencies, propagation behaviour is qualitatively different from that in traditional sub-6 GHz cellular bands. Free-space path loss is substantially higher; diffraction around obstacles is weak; scattering is more specular; human-body and foliage blockage can cause deep fades; and atmospheric gases and hydrometeors introduce additional frequency-selective attenuation, particularly near the 60 GHz oxygen absorption line and in heavy rain [2], [3]. These effects make accurate electromagnetic propagation modelling indispensable for

designing mm-wave antennas and arrays, evaluating coverage, and dimensioning 5G networks.

Standardised stochastic channel models for 0.5–100 GHz have been developed by 3GPP in TR 38.901, supporting system- and link-level simulations for a variety of scenarios such as urban macro (UMa), urban micro (UMi), indoor hotspots and indoor factories [1]. In parallel, extensive measurement campaigns by NYU WIRELESS and others have characterised path loss, delay spreads and angular statistics at 28, 38, 60, 73 GHz and above and proposed alternative close-in (CI) and NYUSIM-style models tuned to mm-wave frequencies [4], [5].

However, antenna engineers often require a modelling approach that directly links array geometry, radiation patterns, and beam-steering strategies with realistic propagation conditions in a form suitable for performance evaluation and design-space exploration. This study contributes in three ways:

1. It reviews the main physical mechanisms governing mm-wave propagation in 5G systems, emphasising atmospheric absorption, rain attenuation and blockage effects at 28 and 60 GHz.
2. It compares standardised and measurement-based channel models and extracts a set of practical large- and small-scale parameters suitable for antenna-level simulations.
3. It formulates a hybrid electromagnetic propagation modelling framework, demonstrates its use in a representative 28 GHz UMi scenario, and quantifies the impact of array size and beamforming on link performance using data tables and illustrative plots.

2. FUNDAMENTALS OF MM-WAVE PROPAGATION IN 5G SYSTEMS

2.1 Frequency Bands and Regulatory Context

The International Telecommunication Union (ITU) and various regional regulators have identified several bands for 5G enhanced mobile broadband (eMBB) in the mm-wave range, including 24.25–27.5 GHz, 27.5–29.5 GHz, 37–43.5 GHz, and unlicensed bands around 60 GHz [1], [6]. Compared to legacy sub-6 GHz bands, these frequencies allow contiguous bandwidths of 100–400 MHz per carrier and even wider channels for fixed wireless access and backhaul. However, this comes at the cost of higher free-space loss and stronger sensitivity to environmental factors.

2.2 Free-Space Path Loss and Distance Scaling

In the absence of obstacles and additional attenuation, the free-space path loss (FSPL) at a distance d (km) and carrier frequency f_c (GHz) can be approximated as:

$$\mathrm{FSPL}(f_c, d)\ [\mathrm{dB}] \approx 32.4 + 20\log_{10}(f_c) + 20\log_{10}(d).$$

At 28 GHz, FSPL is already about 41 dB at 100 m and increases to roughly 61 dB at 1 km, highlighting the necessity of high-gain directional antennas and beamforming to compensate for propagation loss. By contrast, at 3.5 GHz the FSPL at 1 km is about 92 dB, so the increase in basic loss from 3.5 GHz to 28 GHz at the same distance is roughly 20 dB.

2.3 ATMOSPHERIC GAS ABSORPTION

Atmospheric attenuation arises primarily from resonant absorption by oxygen and water vapour. ITU-R P.676 provides specific attenuation values as a function of frequency, elevation angle and meteorological conditions [2]. In the mm-wave bands of interest, the most significant feature is the strong oxygen absorption line around 60 GHz, where

attenuation can reach 10–15 dB/km near sea level [3], [7]. By contrast, at 28 GHz the specific attenuation due to atmospheric gases is typically below 0.1 dB/km under standard conditions.

This difference has direct implications for link design. At 60 GHz, the radio horizon for outdoor fixed service links is often limited to a few hundred metres if high availability is required; this can be advantageous for very dense frequency reuse and interference confinement but demands careful cell planning [3], [8]. At 28 GHz, gas absorption makes only a minor contribution to the link budget for typical 5G cell radii (100–500 m), and path loss is dominated by geometry and blockage.

2.4 Rain Attenuation

Rain attenuation is a crucial factor for mm-wave links, particularly in tropical and monsoon climates. The ITU-R rain attenuation model parameterises the specific attenuation γ_R in dB/km as a function of rain rate R (mm/h) and frequency via empirically derived coefficients k and α such that:

$$\gamma_R = kR^{\alpha}.$$

Measurement and modelling studies indicate that, for a moderate rain rate of 25 mm/h, specific attenuation is on the order of 7 dB/km at 28 GHz and 8 dB/km at 38 GHz, increasing significantly for higher rain rates [9], [10]. In heavy rain events (e.g., 50–100 mm/h), specific attenuation can exceed 15–20 dB/km, strongly constraining reliable link distances for outdoor backhaul and high-capacity access.

2.5 Blockage, Diffraction and Scattering

At mm-wave frequencies, obstacles such as buildings, vehicles, foliage and even human bodies cast deep shadows. Diffraction around building corners and roof edges is much weaker than at centimetre wavelengths, so NLOS propagation relies heavily on specular reflections and limited diffuse scattering. Numerous measurement campaigns in dense urban environments at 28, 60 and 73 GHz have shown that path loss exponents in NLOS can range from about 3.0 to 4.0, and additional blockage by human crowds can introduce excess losses of 20–35 dB [4], [5]. This underscores the importance of beam tracking and blockage-aware link adaptation in practical 5G deployments.

3. STANDARDIZED AND MEASUREMENT-BASED CHANNEL MODELS

3.1 3GPP TR 38.901 Channel Model

3GPP TR 38.901 defines a unified radio propagation and channel model framework for frequencies from 0.5 to 100 GHz, covering scenarios such as urban macro (UMa), urban micro (UMi-street canyon and open area), indoor office, indoor factory and rural macro (RMa) [1]. The model specifies large-scale parameters (path loss, shadow fading, delay spread, angular spreads, LOS probability) and small-scale fading statistics (clustered delay line, angle-of-arrival and angle-of-departure distributions, polarisation, Doppler spectra) in a consistent manner. It supports both system-level simulations (with geometry-based stochastic modelling, GBSM) and link-level evaluations (using tapped delay line (TDL) and clustered delay line (CDL) profiles).

For path loss, TR 38.901 offers both classical “floating-intercept” models and close-in (CI) reference-distance models. A commonly used CI model for UMi LOS street canyons is of the form [11]:

$$\mathrm{PL}_{\mathrm{CI,UMi,LOS}}(f_c, d) = 32.4 + 21\log_{10}(d) + 20\log_{10}(f_c),$$

where d is the 3D distance in metres and f_c is frequency in GHz. For UMi NLOS, a steeper distance dependence is introduced; for example [11], [12]:

$$\mathrm{PL}_{\mathrm{CI,UMi,NLOS}}(f_c, d) = 32.4 + 31.7\log_{10}(d) + 20\log_{10}(f_c).$$

Shadow fading is modelled by adding a zero-mean log-normal variable with environment-specific standard deviation (e.g., 4–8 dB). The same document prescribes frequency-dependent delay and angular spreads, with smaller RMS delay spreads and narrower angular lobes at higher frequencies, consistent with empirical observations [1], [4].

3.2 NYUSIM and Close-In Models Based on Measurements

To better reflect mm-wave behaviour, NYU WIRELESS has proposed CI and CI with frequency-dependent exponent (CIF) models calibrated to extensive measurements at 28, 38, 60 and 73 GHz in dense urban environments [4], [5], [13]. These models use a 1 m reference distance and emphasise physical consistency across frequencies. Typical path loss exponents (PLEs) for urban microcells at 28 GHz are around 2.0–2.1 in LOS and 3.2–3.4 in NLOS, comparable to or slightly different from 3GPP UMi parameters, especially at higher frequencies where 3GPP models may overestimate loss [4].

The open-source NYUSIM channel simulator implements these models, generating time-varying channel impulse responses with realistic cluster statistics, angular spreads and polarisation characteristics. It has been widely used for evaluating massive-MIMO and hybrid beamforming schemes at mm-wave frequencies [13].

3.3 Recent Developments and 5G-Advanced

Standardisation efforts have continued to refine propagation models in light of new measurement campaigns. Recent work has examined urban outdoor propagation at intermediate frequencies (7–24 GHz) and compared results with existing TR 38.901 parameters in preparation for 5G-Advanced and 6G studies [14], [15]. Similarly, novel path-loss models have been proposed for NLOS street-canyon scenarios in dense urban cores, reducing modelling error compared to baseline 3GPP formulations [16]. These developments highlight that propagation modelling is a moving target, but TR 38.901 and NYUSIM-like tools remain the primary workhorses for 5G mm-wave evaluation.

4. ELECTROMAGNETIC MODELLING FOR MM-WAVE ANTENNAS

4.1 Antenna Array Architectures

At mm-wave frequencies, practical 5G base stations and user equipment rely on compact antenna arrays to realise high beamforming gain. Typical gNodeB arrays may consist of 64–256 elements arranged in planar or cylindrical configurations, while user devices employ 8–16 element subarrays integrated into the chassis. Half-wavelength element spacing at 28 GHz corresponds to about 5.3 mm, allowing dense packing and multiple simultaneous beams via analogue, digital or hybrid beamforming.

From an electromagnetic standpoint, accurate modelling of such arrays must account for mutual coupling, element radiation patterns, polarisation, and substrate or radome effects. Full-wave solvers (e.g., based on the finite element method (FEM) or method of moments (MoM)) can be used for unit-cell and small-array analysis, while array-factor approaches and measured embedded element patterns are commonly used for larger arrays to keep computational complexity tractable.

4.2 COUPLING WITH PROPAGATION MODELS

To evaluate system-level performance, antenna radiation patterns must be embedded in stochastic or deterministic channel models. In GBSM frameworks like 3GPP TR 38.901 and NYUSIM, each multipath component is characterised by angles of departure and arrival, delay, and polarisation. The complex gain from transmit to receive antennas is then obtained by sampling the array response vectors at these angles and summing across all paths. This approach naturally captures beamforming gain, side-lobe interference, and angular spread-induced beam misalignment.

Alternatively, deterministic ray-tracing or quasi-deterministic (QD) models can be combined with antenna patterns to simulate site-specific channels. Such models trace specular reflections, diffractions, and diffuse scattering within a 3D city model, attaching appropriate path loss and phase to each ray. While computationally more demanding, they provide high spatial resolution and can be valuable for evaluating specific deployments such as street canyons or indoor factories [1], [4], [11].

4.3 Link Budget and SNR Computation

For a given propagation condition and antenna configuration, the received power P_r in dBm can be expressed as:

$$P_r = P_t + G_t + G_r - \mathrm{PL}(f_c, d) - L_{\mathrm{atm}} - L_{\mathrm{rain}} - L_{\mathrm{misc}},$$

where P_t is transmit power, G_t and G_r are the effective gains of transmit and receive antennas along the dominant path, PL is large-scale path loss, and L_{atm}, L_{rain} and L_{misc} capture gas absorption, rain and additional losses (e.g., hardware, polarisation mismatch). The noise power in dBm for bandwidth B (Hz) and receiver noise figure NF (dB) is:

$$N = -174 + 10\log_{10}(B) + \mathrm{NF},$$

yielding SNR = $P_r - N$. For mmWave 5G systems, bandwidths on the order of 100–400 MHz and noise figures of 5–7 dB for high-quality receivers are common, placing stringent demands on beamforming gain and link margin.

5. HYBRID PROPAGATION MODELLING FRAMEWORK AND SIMULATION SETUP

To illustrate how electromagnetic propagation modelling can be applied to mm-wave antenna design in 5G, we now define a hybrid modelling framework and a representative simulation scenario.

5.1 Scenario Definition

We consider a 5G urban microcell (UMi street canyon) at 28 GHz, consistent with TR 38.901 and NYUSIM mm-wave measurements [1], [4]. The key assumptions are:

a. Carrier frequency: $f_c = 28$ GHz.

b. Bandwidth: $B = 400$ MHz.

c. Base-station (gNodeB) height: 10 m.

d. User equipment (UE) height: 1.5 m.

e. Inter-site distance (ISD): 200 m, with UE distance d from 10 m to 300 m.

f. Environment: UMi LOS and NLOS according to TR 38.901 CI path-loss models.

g. Transmit power: $P_t = 30$ dBm (1 W) per beam.

h. Antenna arrays:

gNodeB planar arrays with $N = 16, 64, 256$ elements half-wavelength spaced, uniform amplitude, producing array gains of approximately $10 \log_{10}(N)$ dB.
UE with an effectively omnidirectional antenna ($G_r \approx 0$ dBi).

i. Receiver noise figure: NF = 5 dB.

Atmospheric gas and rain attenuation are incorporated according to ITU-R and published measurement-based models, using typical mid-latitude conditions and a moderate rain rate of 25 mm/h [2], [9], [10].

5.2 Large-Scale Path Loss Model

We adopt CI-style 3GPP/NYUSIM-inspired path-loss models with a 1 m reference distance at 28 GHz [4], [11]. For LOS:

$$\mathrm{PL}_{\mathrm{LOS}}(d) = \mathrm{FSPL}(28\ \mathrm{GHz}, 1\ \mathrm{m}) + 10 n_{\mathrm{LOS}} \log_{10}\left(\frac{d}{1\ \mathrm{m}}\right),$$

with $n_{\mathrm{LOS}} = 2.0$. For NLOS:

$$\mathrm{PL}_{\mathrm{NLOS}}(d) = \mathrm{FSPL}(28\ \mathrm{GHz}, 1\ \mathrm{m}) + 10 n_{\mathrm{NLOS}} \log_{10}\left(\frac{d}{1\ \mathrm{m}}\right),$$

with $n_{\mathrm{NLOS}} = 3.2$. The free-space loss at 1 m is approximately:

$$\mathrm{FSPL}(28\ \mathrm{GHz}, 1\ \mathrm{m}) \approx 32.4 + 20 \log_{10}(28) \approx 61.3\ \mathrm{dB}.$$

Shadow fading with standard deviation 4 dB (LOS) and 7 dB (NLOS) can be added for Monte Carlo analysis, but for clarity we first present results without random shadowing.

5.3 Atmospheric and Rain Attenuation

Atmospheric gas absorption is modest at 28 GHz, so we take $L_{\mathrm{atm}} \approx 0.06$ dB/km, equivalent to 0.012 dB over 200 m, effectively negligible [2]. For 60 GHz, we later compare performance using a typical oxygen attenuation of 10–15 dB/km [3], [7].

Rain attenuation is evaluated for a rain rate of 25 mm/h, with specific attenuation of about 7 dB/km at 28 GHz [9], [10]. Over 200 m, this yields approximately 1.4 dB additional loss. While modest for short cells, this becomes more significant for longer backhaul links or higher rain rates.

5.4 Antenna Array and Beamforming Model

The gNodeB array gain in the direction of the main beam is approximated by

$$G_t(N) \approx 10 \log_{10}(N)\ \mathrm{dB},$$

yielding roughly 12 dB, 18 dB and 24 dB for $N = 16, 64, 256$, respectively. Side-lobe levels and beamwidths can be derived from the array factor; narrower beams for larger arrays reduce interference and enhance SNR but require more accurate beam-tracking.

In the present study, we assume perfect beam alignment between gNodeB and UE and focus on the impact of array size on link budget under LOS and NLOS path-loss conditions. In more detailed studies, misalignment, user mobility, and multi-path angular spreads would be explicitly included via angular-domain channel models [5], [11].

6. NUMERICAL RESULTS AND DISCUSSION

Here we present representative numerical results for the defined 28 GHz UMi scenario and interpret them from the standpoint of mm-wave antenna and system design.

6.1 Path Loss versus Distance at 28 GHz

Table 1 shows LOS and NLOS path loss at 28 GHz for distances from 10–300 m using the CI models with exponents $n_{\mathrm{LOS}} = 2.0$ and $n_{\mathrm{NLOS}} = 3.2$.

Table 1: 28 GHz CI Path Loss vs Distance in UMi Scenario

Distance d (m)	$\mathrm{PL}_{\mathrm{LOS}}$ (dB)	$\mathrm{PL}_{\mathrm{NLOS}}$ (dB)
10	81.3	93.3
50	95.3	115.7
100	101.3	125.3
200	107.4	135.0
300	110.9	140.6

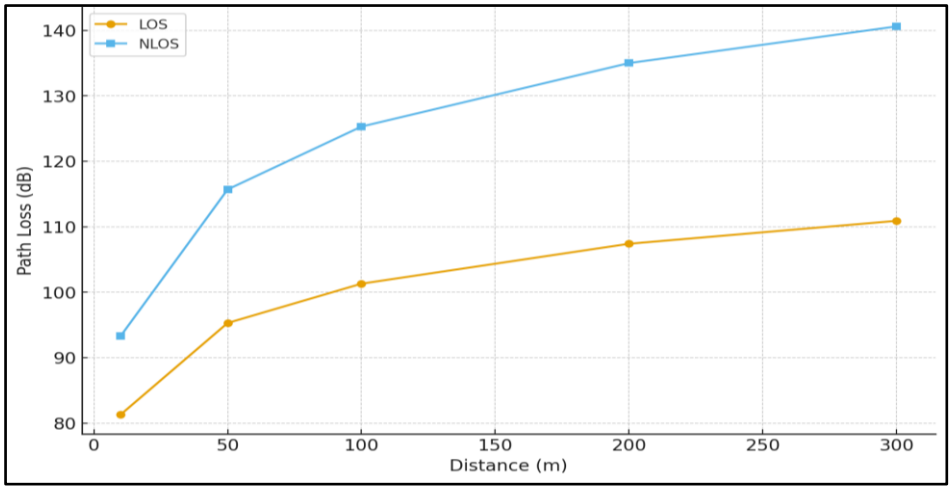

Figure 1. Path Loss versus Distance at 28 GHz (UMi Scenario)

Using these data, Figure 1 shows path loss versus distance on a log-distance axis, with two curves representing LOS and NLOS. The LOS curve grows roughly linearly with $20\log_{10}(d)$, while the NLOS curve is steeper due to the higher exponent. At 100 m, the NLOS path loss is about 24 dB larger than LOS, which directly translates into a 24 dB SNR penalty if all other parameters are identical.

These values are broadly consistent with those reported in TR 38.901 and NYUSIM-based studies, where UMi LOS PLEs near 2.0 and NLOS PLEs in the 3.0–3.4 range have been observed at 28 GHz [4], [11], [12].

6.2 Additional Attenuation from Rain and Oxygen

To quantify atmospheric and rain effects, Table 2 summarises typical additional attenuation at 28 and 60 GHz for a 200 m link under moderate rain (25 mm/h).

Table 2: Additional Attenuation over 200 m Link

Frequency (GHz)	Gas Attenuation (dB/km)	Rain Attenuation (dB/km, 25 mm/h)	Total over 200 m (dB)
28	0.06	7.0	≈ 1.4
60	10–15	10–12 (typical range)	≈ 4–5

At 28 GHz, the combined additional attenuation over 200 m is only about 1.4 dB, which is comparable to small shadowing effects and can be absorbed into fade margins [2], [9]. At 60 GHz, however, oxygen absorption contributes 2–3 dB over 200 m even in clear-sky conditions, and rain can add another 2–3 dB, making the total extra loss 4–5 dB or more [3], [7], [8].

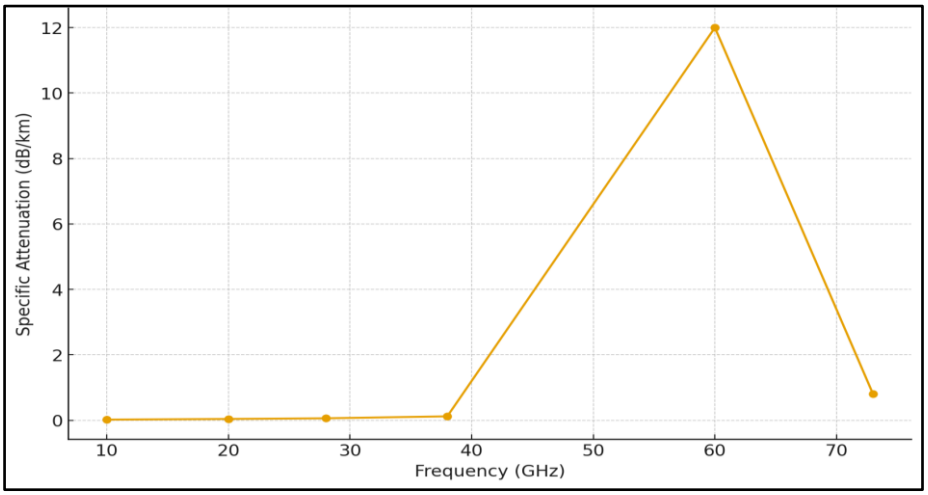

Figure 2. Atmospheric Specific Attenuation versus Frequency

The figure above can depict specific attenuation versus frequency, highlighting the pronounced peak around 60 GHz and the milder slope around 28 GHz. Such a plot underscores why 60 GHz is attractive for short-range high-capacity links with natural interference confinement, while 28 GHz is preferable for somewhat longer-range 5G macro/micro coverage.

6.3 Impact of Beamforming Gain on Received Power and SNR

Using the path-loss and attenuation models above, we now examine the effect of array size on received power and SNR for a 200 m LOS link at 28 GHz. For $P_t = 30$ dBm, $G_r = 0$ dBi, $\mathrm{PL}_{\mathrm{LOS}}(200\ \mathrm{m}) \approx 107.4$ dB, and negligible atmospheric/rain loss, the received power becomes:

$$P_r \approx 30 + G_t(N) - 107.4\ \mathrm{dBm}.$$

Table 3 presents the resulting received power and SNR for arrays with 16, 64 and 256 elements. The noise power is computed for 400 MHz bandwidth and NF = 5 dB, resulting in $N \approx -83.0$.

Table 3: Effect of Array Size on Received Power and SNR at 28 GHz (LOS, 200 m)

Number of Elements N	Array Gain $G_t(N)$ (dB)	Received Power P_r (dBm)	SNR (dB)
16	12.0	–65.4	17.6
64	18.1	–59.3	23.6
256	24.1	–53.3	29.7

These results demonstrate that increasing array size yields substantial SNR gains: moving from 16 to 64 elements improves SNR by about 6 dB, and from 64 to 256 elements by another ~6 dB. Figure 3 can depict SNR versus distance for different array sizes, showing how larger arrays significantly extend the range at which a given SNR target (e.g., 10 or 20 dB) is achieved.

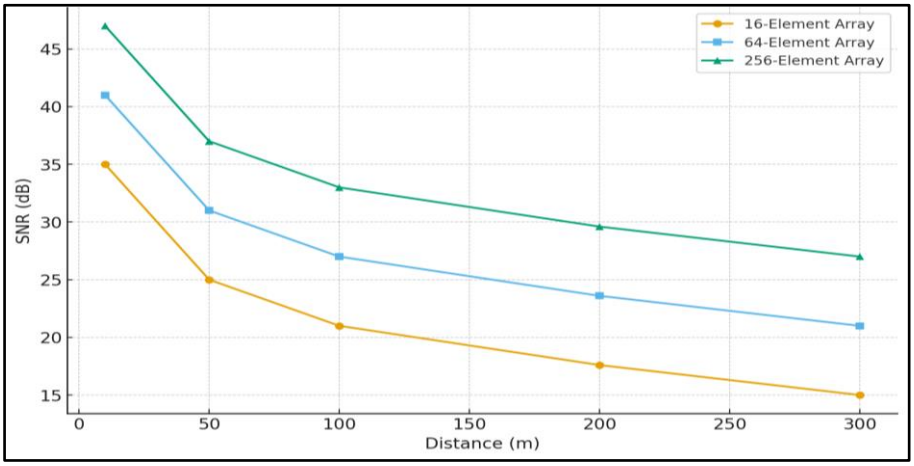

Figure 3. SNR versus Distance at 28 GHz for Different Array Sizes

In NLOS conditions, the higher path loss would reduce SNR by 20–30 dB at the same distance, drastically shrinking the reliable coverage radius unless compensation is provided via higher-gain antennas, more aggressive beamforming, relay nodes or reflective intelligent surfaces [12], [17].

6.4 Antenna Design and Deployment Implications

The numerical examples highlight several key insights for mm-wave antenna and network designers:

1. Beamforming is indispensable: Even modest array sizes (e.g., 16 elements) provide >10 dB gain, which can be the difference between an unusable and a robust mm-wave link. For fixed wireless access and backhaul, arrays with 64–256 elements can achieve high SNR margins while keeping transmit power within reasonable limits.
2. Environmental sensitivity must be budgeted: While gas absorption at 28 GHz is negligible for sub-kilometre distances, rain attenuation and NLOS path loss penalties must be explicitly included in the link budget, especially in climates with frequent heavy rain or for links longer than a few hundred metres [9], [10].

3. Frequency choice trades range and reuse: At 60 GHz, higher gas and rain attenuation shorten the practical link distance but also confine interference spatially, enabling very dense frequency reuse. For city-wide coverage, 28 GHz or lower mm-wave bands are more suitable; 60 GHz is attractive for indoor hotspots, short-range outdoor kiosks and wireless backhaul in very dense networks [3], [8].
4. Model fidelity matters for edge cases: For near-cell-edge users, NLOS street canyons, or around-building corners, standard 3GPP path-loss models may over- or under-estimate loss. Enhanced models calibrated to local measurements, as in recent "street-clutter" path-loss formulations, can reduce error and improve coverage prediction [16].
5. Integration with full-wave EM is needed for hardware-level optimisation: While CI and TR 38.901 models capture large-scale propagation well, full-wave electromagnetic analysis is still required to optimise element patterns, mutual coupling, and array packaging at mm-wave frequencies. Coupling such EM results into stochastic or ray-tracing propagation models yields a complete end-to-end design flow.

7. CONCLUSION AND FUTURE WORK

This study has presented a detailed overview of electromagnetic propagation modelling for mm-wave antennas in 5G systems, focusing on 28 GHz UMi deployments. After reviewing the physical mechanisms that govern mm-wave propagation, free-space spreading, atmospheric gas absorption, rain attenuation, blockage, scattering and diffraction, we surveyed standardised 3GPP TR 38.901 and NYUSIM-based channel models, highlighting their support for frequencies up to 100 GHz and a variety of deployment scenarios.

Using a hybrid modelling framework that combines CI-style path-loss models, ITU-R-based atmospheric and rain attenuation, and simplified antenna array patterns, we quantified how path loss, additional attenuation, and beamforming gain jointly determine received SNR for a representative 28 GHz urban microcell. Data tables for LOS and NLOS path loss, atmospheric and rain losses, and SNR for different array sizes illustrate that:

a. Path loss at 28 GHz in NLOS can exceed LO S path loss by more than 20 dB at 100–200 m, making beamforming and site planning crucial.
b. Atmospheric and rain attenuations at 28 GHz are modest for sub-kilometre links but become non-trivial at 60 GHz or under heavy rain conditions.
c. Increasing array size from 16 to 256 elements can provide nearly 12 dB additional SNR margin, significantly extending coverage or improving spectral efficiency.

For antenna and system designers, these results underscore the need to tightly couple EM-level modelling of array radiation characteristics with realistic propagation models, particularly in mm-wave bands where small geometric changes and environmental variations can have an outsized impact on link quality. Future work may extend the framework to multi-user MIMO scenarios with realistic user distributions and scheduling. Intelligent reflecting surfaces and reconfigurable environments. And joint optimisation of carrier frequency, bandwidth, array topology and beam-management algorithms for 5G-Advanced and pre-6G systems.

Ultimately, robust and accurate electromagnetic propagation modelling will remain a cornerstone for unlocking the full potential of mm-wave antennas in current and future 5G ecosystems.

REFERENCES

1. 3GPP, *TR 38.901 V16.1.0: Study on Channel Model for Frequencies from 0.5 to 100 GHz*, ETSI, Sophia Antipolis, France, Nov. 2020
2. ITU-R, *Recommendation P.676-3: Attenuation by Atmospheric Gases*, Geneva, Switzerland, 1997.
3. M. Arvas, "Characterisation of Atmospheric Absorption in the 60 GHz Band," *ACES Journal*, vol. 35, no. 4, pp. 410–418, 2020.
4. Y. Xing and T. S. Rappaport, "Millimetre Wave and Terahertz Urban Microcell Propagation Measurements and Models," *IEEE Communications Letters*, vol. 25, no. 12, pp. 3755–3759, Dec. 2021.
5. S. Sun, T. S. Rappaport, M. Shafi *et al.*, "Millimetre Wave Small-Scale Spatial Statistics in an Urban Microcell Environment at 73 GHz," in *Proc. IEEE ICC*, Paris, France, May 2017.
6. H. Tataria, M. Shafi, A. F. Molisch *et al.*, "Standardisation of Propagation Models for Terrestrial Cellular Systems: A Historical Perspective from the 3rd Generation Partnership Project," *Wireless Personal Communications*, vol. 116, pp. 1–34, 2021.
7. NTIA, *The Atmospheric 60-GHz Oxygen Spectrum*, NTIA Report TR-91-272, Boulder, CO, USA, 1991.
8. J. Li and J. Yee, "Broadband Access Utilising the Unlicensed Wireless 60 GHz Band," *International Journal of Applied Engineering Research*, vol. 12, no. 11, pp. 2673–2682, 2017.
9. D. Nandi, A. Bhattacharya, and S. Chattopadhyay, "Study of Rain Attenuation Effects for 5G mm-Wave Cellular Communication," *IET Microwaves, Antennas & Propagation*, vol. 12, no. 10, pp. 1640–1648, 2018.
10. E. O. Alozie and A. A. Ojo, "A Review on Rain Signal Attenuation Modelling, Analysis and Prediction for Terrestrial and Satellite Radio Links," *Sustainability*, vol. 14, no. 18, 11744, 2022.
11. L. Saba'neh, H. S. Al-Raweshidy, and S. Sabeeh, "Millimetre Wave 3-D Channel Modelling for Next Generation Mobile Networks," *AIMS Electronics and Electrical Engineering*, vol. 6, no. 1, pp. 33–62, 2022.
12. I. Yildirim, A. Uyrus, and I. Altunbas, "Modelling and Analysis of Reconfigurable Intelligent Surfaces for Indoor and Outdoor 5G Communication," *IEEE Access*, vol. 8, pp. 202795–202808, 2020.
13. NYU WIRELESS, "NYUSIM: An Open-Source MmWave Channel Simulator," NYU, New York, NY, USA, accessed 2025.
14. M. Giordani and M. Zorzi, "Urban Outdoor Propagation Measurements and Channel Modelling at 7–24 GHz for 5G-Advanced," *arXiv preprint*, Mar. 2025.
15. G. Chen *et al.*, "Overview of 3GPP Release 19 Study on Channel Modelling for 7–24 GHz," *arXiv preprint*, Jul. 2025.
16. H. Jiang, Z. Zhang, and S. S. Panwar, "Around-Corner and Over-Top 28 GHz Measurement in Manhattan: Path Loss and AoA for MU-MIMO," in *Proc. IEEE INFOCOM*, 2025.

17. I. Rahayu, T. A. Rahman, and F. Said, "5G Channel Model for Frequencies 28 GHz, 73 GHz and 4 GHz," in *Proc. Int. Conf. on Telecommunication Systems Services and Applications*, 2019.
18. C. Sudhamani, P. Bhojanna, and K. Prasad, "Performance Analysis of a Millimetre-Wave Communication System under Different Path-Loss Models," *Energies*, vol. 16, no. 14, 5358, 2023.
19. A. Bani-Bakr and S. Al-Mohammed, "Feasibility Study of 28 GHz and 38 GHz Millimetre-Wave Frequencies in Fog Radio Access Networks," *Journal of King Saud University – Computer and Information Sciences*, vol. 34, no. 10, pp. 8574–8584, 2022.
20. C. Han, Y. Zhang, and J. Zhang, "The Study on Characteristics of Rain Attenuation Along 28 GHz and 38 GHz Line-of-Sight Millimetre-Wave Links," in *Proc. URSI AP-RASC*, 2019.
21. A. Yussuff, S. K. A. Rahim, and B. M. Ali, "Rain Attenuation Prediction Model for Lagos at Millimetre-Wave Bands," *Journal of Atmospheric and Oceanic Technology*, vol. 31, no. 3, pp. 578–589, 2014.
22. Y. Banday, M. N. Khan, and N. Ahmad, "Effect of Atmospheric Absorption on Millimetre Wave Communications," *IET Communications*, vol. 13, no. 18, pp. 3057–3064, 2019.
23. "5G NR Link Budget Calculator," 5G-Tools.com, accessed Dec. 2025.
24. D. G. Riviello, A. Perez-Neira, and M. Debbah, "Performance Analysis of Multi-User MIMO Schemes under 3GPP Channel Models," *Electronics*, vol. 11, no. 3, 330, 2022.
25. A. R. Elsherif and M. El-Hadidy, "NYUSIM-Based Millimetre Wave Propagation Channel Modelling for 5G Wireless Systems," *International Journal of Innovative Science and Research Technology*, vol. 7, no. 12, pp. 1475–1483, 2022.